2D-IMAGING OF THE EFFECTS FROM FRACTURES ON OIL RECOVERY IN LARGER BLOCKS OF CHALK

Bjorn G. Viksund[1], Terje Eilertsen[1], Arne Graue[1], Bernard A. Baldwin[2] and Eugene Spinler[2]
[1] University of Bergen, Norway
[2] Phillips Petroleum Co., Oklahoma, USA

ABSTRACT
The effect of fractures on the movement and recovery of hydrocarbons from large blocks of strongly water-wet chalk has been studied in the laboratory using 2-D nuclear tracer saturation imaging. The objectives of the experiments were to study the impact of fractures on fluid flow mechanisms, total oil recovery, distribution of residual oil and to evaluate the effect of capillary continuity across the fractures.

Tracking the water flow paths in constant pressure and constant rate waterfloods on whole and then fractured chalk blocks showed that brine imbibition of the whole block occurred as a gradual uniform increase in brine saturation throughout the block with high initial water saturation, while frontal advancement of a water bank was observed with lower initial water saturation. The fractures in the blocks impeded and redirected the flow of water but total oil recovery was similar for fractured and unfractured blocks. In general, no fracture was crossed until the preceding matrix was nearly at final water saturation. Gravity segregation of fluids in open fractures was identified and had a significant impact on the flow pattern. Repeatability of the waterflood in the fractured blocks was very good.

INTRODUCTION
The oil production mechanism in fractured water-wet chalk has long been believed to be governed by spontaneous imbibition from water filled fractures and movement of the expelled oil into and through the fractures to the production well. However, with sufficient capillary contact between the matrices on either side of a fracture some oil may also move through the matrix. Thus, viscous displacement of oil may play a role, especially during waterfloods and in reservoirs which are less than highly water-wet. To assess this issue, a series of experiments has been reported on the impact of fractures on hydrocarbon displacement mechanisms. Spontaneous axial imbibition in stacked cores has been monitored in horizontal and vertical configurations using a dynamic in-situ, nuclear tracer imaging technique. In addition the scaling of oil recovery by spontaneous imbibition and waterflooding in cores of various lengths and areas of the exposed faces, i.e. 1-D, 2-D and 3-D exposure, the gravitational effects on vertically stacked cores and the impact of the presence of gas have been investigated (Ref. 1,2,3,4). Experiments have also been performed to alter the wettability of outcrop chalk and produce a porous rock which mimics the reservoir rock during laboratory studies (Ref. 5).
This paper investigates fluid movement and hydrocarbon recovery mechanisms in blocks of highly water-wet outcrop chalk from the Dania and Rørdal outcrops in Denmark, containing embedded fractures. Open, "closed", horizontal and vertical fractures were included in the blocks to study how the orientation and width affected the fluid flow (Ref. 6). We report on how a) different fractures, and b) constant injection rate and constant differential pressure, affected the flow of fluids in fractured chalk blocks.

EXPERIMENTAL

Three blocks, approximately 20 cm × 12 cm × 5 cm, were cut from large pieces of outcrop chalk. This material was highly water-wet. Each block was oven dried for three days at 90° C, end pieces were mounted and the whole assembly was epoxy coated. Each end piece contained three fittings at the inlet and outlet to help distribute injected and produced fluids. Each block was vacuum evacuated and saturated with brine containing 5 wt% NaCl + 5 wt% $CaCl_2$. Porosity was determined from weight measurements and the permeability was measured across the epoxy coated block, see Table 1.

Before the block was epoxy coated, local air permeability was measured on both sides of the blocks using a minipermeameter. Permeability measurements were made at each intersection of a 2 cm × 2 cm grid across the surface, for both the front and back sides of the blocks. One example map of the air permeability distribution is shown in Figure 1. Similar homogeneous permeability maps were obtained for the other blocks.

2-D brine saturations were determined using a flow rig, designed and built at the University of Bergen, to measure gamma ray emission from ^{22}Na dissolved in the brine. The rig held the block in a vertical position and measured the radiation in the x-y plane over the block to produce a saturation map at each specified point in time. The working principle of the imaging technique has been described in detail (Ref. 7, 8). The detector was collimated to produce an analysis area of 1 cm × 1 cm at the surface of the block which expanded to 1.8 cm × 1.8 cm at the back of the block giving an analysis volume of 9.8 cm^3. In order to avoid bypass between the block and the epoxy coating (Ref. 6) one of the blocks, Block CHP-6, was placed in a pressure vessel and confinement pressure was applied during the waterflood. Because of the additional pressure vessel the distance to the detector increased and the analysis volume increased accordingly to 36.7 cm^3.

The radiation counting time at each position was 3 minutes, giving a total sampling time, for one 2 cm × 2 cm saturation scan, of 2 hours and 45 minutes. The change in saturation during this time, less than 0.03 PV, is small compared to the volume needed to produce a noticeable change in the saturation map. Thus, no correction was made to account for the saturation change during the sampling time.

The individual saturation maps are identified by scan numbers. The code for the scans are as follows: The radioactive brine displacing non-radioactive brine were labeled M, for a miscible flood, and 1 for being the first one. The numbers following the dash indicate the chronological sequence of the scans. The oil and water floods were labeled O and W, respectively, with the first digit being the flood number and the two digits following the dash indicating the chronological sequence of scans. Thus, M1-03 is the 3rd scan in the 1st miscible flood, W2-09 is the 9th scan of the 2nd water flood and O2-02 is the 2nd scan of the 2nd oil flood. Each scan number representing the individual saturation maps, was preceded by a letter and a number to identify each block, for example P2, P5 and P6 for CHP-2, CHP-5 and CHP-6, respectively.

In all the waterflood experiments the brine was injected from the left side of the image and the displaced fluids exited at the right side of the image. For oilflood, to achieve S_{wi}, decane was alternately injected in both ends.

The blocks were cut to size with a band saw and used without cleaning. The fractures were created, after the first water flood when the whole block had been driven back to S_{wi}, by cutting the blocks CHP-4 and CHD-1 with a hand saw and block CHP-6 with a band saw. The reason different saws

were used was to create fractures with different surface roughness to produce different capillary continuity and fracture permeability. Although the cut blocks from CHD-1 were placed next to each other for the "closed" fractures no force was applied to mechanically hold them in position. The cut blocks from CHP-4 and CHP-6 were placed next to each other for the "closed" fractures and a force producting a pressure of 0.1 bar across the fractures, was applied to mechanically hold them in position. The fracture orientation and location for CHD-1 are shown in Figure 2. When reassembling the blocks, tape was placed over the fractures to prevent the epoxy, used to reseal the core, from entering the fractures. A 2 mm strip of Teflon was placed at the outer, lower, edge of the open fracture to assure a well defined open volume.

Decane was used as the hydrocarbon and had an isotopic purity of >95 %. Oilfloods of the epoxy coated blocks, to drive the core to S_{wi}, were carried out in a separate pressure vessel which was capable of holding up to 30 bars (450 psi) of confining pressure so that a maximum pressure drop of 25 bars (375 psi) could be applied across an epoxy coated block.

To prevent counter current imbibition from producing oil into the water inlet, a low differential pressure, initially < 15 mbar, was applied across the block during the waterfloods. The injection rates are included in Table 1.

The experimental sequence and results from waterflooding the unfractured and fractured blocks, while using 2-D imaging to determine the distribution of brine saturation, is summarized in Table 1.

RESULTS AND DISCUSSION

Figure 2 is a diagram of the arrangement of the individual pieces in the designed fracture network for CHD-1 after the cut block was reassembled. The xy coordinates are used for location. For reference, the individual blocks are identified as Block A, the inlet block, Block B, the central block which is surrounded by fractures and Block C, the outlet block. Both an open fracture, no possible capillary contact, and horizontal and vertical "closed" fractures, with contact between the adjacent matrix blocks, were formed. The "closed" fractures were intended to provide some capillary continuity of both fluid phases across the fracture. The open vertical fracture at 13 cm was created by sliding Block B to the left as far as possible. This produced an open fracture with the width of one saw cut, ca. 2 mm. The other fractures were "closed", i.e. the pieces were placed butt to butt when reassembling the block. After reassembly the fracture network was filled with decane using a syringe.

In all the figures which show the water/oil displacements, the designation along the x-axis denotes the grid position along the length of the block in cm and the numbers along the y-axis denote the grid position along the height of the block in cm. Radiation detection, i.e. saturation measurement, during the waterflood was made at the odd numbered sites, shown as the circles on Figure 2, a 2 cm x 2 cm grid. For all the blocks CHD-1, CHP-6 and CHP-4 the first vertical fracture is at 4 cm from the inlet end, the second vertical fracture is at 13 cm from the inlet end and the horizontal fracture is in the center line of the block. Due to the difference in overall length of the blocks CHD-1, CHP-6 and CHP-4, the block at the outlet end, after the last vertical fracture, Block C, will have a slightly different length in the three cases. For most of the images at static conditions, end-point saturations, the spatial resolution was increased to 1 cm $\times$ 1 cm by making measurements at every intersection in the grid. The reduced resolution during the dynamic portion of the experiment was required to avoid significant change in the fluid distribution while the radiation measurements were being made.

Although $CaCl_2$ was in the brine to buffer Na adsorption, several pore volumes of non-radioactive brine were initially flushed through the block to minimize potential adsorption of the radioactive tracer, $^{22}NaCl$, before the rock was exposed to the radioactive brine. Injecting radioactive brine the non-radioactive brine was displaced. Saturation maps indicated that an efficient exchange of non-radioactive water by radioactive water took place. Saturation measurements at the end of the flood showed less than 2 % PV saturation variations indicating that the block was homogeneous on a cm scale. These results confirm the constant air permeability measurements.

After the miscible brine-brine displacement an oilflood was performed on each block. The oilfloods were performed in a pressure vessel in order to achieve a high differential pressure across the block. This was necessary in order to obtain a low water saturation. A uniform low water saturation was measured in-situ for all three blocks. The water saturation after the first oilflood on CHP-4 is shown as the first saturation map, P4W1-01, in Figure 3. The measured in-situ saturation gave excellent agreement when compared to the mass balance.

WHOLE BLOCK

Figure 3 shows the waterflood of the whole, unfractured block CHP-4. The water saturation increased as a dispersed front through the block (Figure 3, P4W1-00 - P4W1-19 (Scan P4W1-00 locks different due to a graphical artifact.)). This behavior was also noted for CHP-6 although less dispersed than CHP-4. The waterflood was performed at constant pressure, P=40 mbar corresponding to a initial flow rate of 2.9 cm^3/h and decreasing, in block CHP-4 and at constant flow rate, q=6 cm^3/h, in block CHP-6. Dispersion obviously varied with rate, however, in block CHD-1, q=4 cm^3/h, a rather uniform gradual increase in water saturation was imaged (Ref. 6). This is consistent with Magnetic Resonance Imaging work which showed uniform saturation changes during imbibition, when S_{wi} was high, >30 % (Ref. 9). Under these conditions it appeared that the water relative permeability was high enough to provide water transport through the matrix without the formation of a water bank. The difference in behavior is believed to be caused by the difference in initial water saturation (Table 1).

When the block CHP-4 was driven back to S_{wi} an excellent reproduction of the original water saturation and saturation distribution was obtained, see Table 1 and compare Scan P4W1-01, Figure 3, with Scan P4W2-01 in Figure 4. The measured in-situ saturation was compared to the mass balance and gave excellent agreement. A similar reproducibility was obtained for the other two blocks. The blocks were then cut into the three shapes as shown in Figure 2. The fractures in the reassembled block consisted of two "closed" vertical fractures, one at 4 cm and the upper portion at 13 cm, one open vertical fracture, the lower portion at 13 cm and a "closed" horizontal fracture along the center line of the blocks. The saturation measurements before and after fracturing indicated that the cutting process did not measurably alter the saturation distribution at S_{wi} (Ref. 6).

FRACTURED BLOCK

Constant pressure water flood of Rørdal Block; CHP-4

The scans in Figure 4 show the time development of the 2-D brine saturation during the constant differential pressure, 40 mbar, water flood of the fractured block CHP-4. This was a Rørdal block cut with a hand saw, which gave a coarse surface to the fractures. The brine saturation increased as a dispersed front through Block A, the continuous inlet block, Scans P4W2-01 to P4W2-05. In Scan P4W2-05 Block B was still at, or close to, S_{wi} while the matrix just across the fracture in Block A was approaching S_{wf}. The brine did not appear to cross any of the fractures before the saturation in

all of Block A was close to it's final water saturation. After Block A reached a high water saturation and the fractures were filled with brine, the brine entered Block B, Scan P4W2-06. The general appearance of the saturation distribution in Block B in Scan P4W2-06 suggested that the brine entered gradually from both the horizontal and vertical fractures between Block A and Block B. However, little, if any, water had crossed the 13 cm fracture into Block C at the time when Scan P4W2-07 was taken. When Block B approached it's final water saturation, water movement into Block C, the outlet block, was recorded, scans P4W2-07. A higher water saturation in the lowest part of the Block C at the outlet-end, shown in scan P4W2-07, indicated possible gravity segregation in the open fracture. A prior experiment with Dania outcrop chalk, with the same fracture network, showed a significant effect of gravity in the open vertical fracture (Ref. 6). The reason for this difference can be attributed to a longer time between each individual scan. The vertical intensity bump at 13 cm, Scan P4W3-09, indicated that water collected at the bottom of the open fracture at 13 cm.

A previous constant flow rate water flood experiment on a block of Dania chalk (Ref. 6) showed similar water flow pattern as obtained for the Rørdal block CHP-4. Even though the blocks were constructed from different types of chalk with significantly different matrix permeabilities, k=67 mD and k=2 mD for Dania and Rørdal, respectively, a consistent behavior was observed.

Constant water injection rate of Rørdal Block; CHP-6

The scans in Figure 5 show the time development of the 2-D brine saturation during the constant rate, 1 cm^3/h water flood of the fractured block CHP-6. This was a Rørdal chalk block cut with a band saw, giving fractures with lower surface roughness. The brine saturation increased as a dispersed front through Block A, the continuous inlet block, Scans P6W2-01 to P6W2-20. In Scan P6W2-20 Block B was still at, or close to, S_{wi} while the matrix just across the fracture in block A was approaching S_{wf}. This occurred even though the fractures had significantly less rough and uneven surfaces than for CHP-4. The brine did not appear to cross any of the fractures before the saturation in all of Block A was close to it's final water saturation. The general appearance of Block B in Scan P6W2-24 suggested that the brine entered gradually from both the horizontal and vertical fractures between Block A and Block B. However, little, if any, water had crossed the 13 cm fracture into Block C at the time when Scan P6W2-30 was taken. When Block B approached it's final water saturation, water movement into Block C, the outlet block, was recorded, scans P6W2-34. A higher water saturation in the lowest part of the Block C at the outlet-end, shown in scan P6W2-34, indicated a gravity segregation in the open fracture, as was also indicated for the fracture with coarse surfaces, CHP-4 and CHD-1 (Ref. 6).

Figure 6 shows the effluent profiles from the constant flow rate water floods including results from block CHD-1 in Ref. 6. The oil recovery in the unfractured configuration was almost the same as the fractured configuration, the initial water saturation being equal, even though the flow paths were considerably different in the two cases. Figure 7 shows the effluent profiles from the constant differential pressure water floods. This figure also confirm that the oil recovery in the unfractured configuration was similar to the fractured configuration. There was a slight difference in recovery efficiency between the constant rate and constant pressure cases with the higher recovery observed in the constant rate case. This may be due to the fact that the waterflood at such a low differential pressure, as used in the constant pressure case, was a very slow process, and we suspect that continuing the constant pressure experiment for a longer period of time would have resulted in a recovery efficiency equal to the constant flow rate case.

The pattern of water movement during the water flood of the fractured blocks indicated that there was little capillary contact, for the water phase, between Blocks A and C across the upper portion of the fracture at 13 cm. This behavior was observed for both smooth and coarse fracture surfaces. If there had been significant capillary continuity of the water phase, water would have been expected to readily flow across the fracture and saturate the upper portion of Block C during the early stages of waterflood into Block A. These results suggest that the two blocks were not in physical contact or it suggests that if there was physical contact between the two blocks the amount of capillary continuity of the water phase was insignificant. Reassembly of the original block CHD-1 did not have pressure exerted to ensure good contact of the "closed" fractures. The two other blocks, CHP-4 and CHP-6, were reassembled using a pressure of 0.1 bar to ensure physical contact in the "closed" fractures between the blocks.

During oil movement the oil could flow out of Block A and push the oil, which was already in the fracture, into Block C. Water which entered the fracture may gravity segregate to the bottom. A more prominent effect of the fractures was observed when the flow rate was increased. This is indicated by comparing the saturation maps in Figure 4 and Figure 5 and in Ref. 6.

Due to the fact that the fractures in CHP-4 and CHP-6 were generated by different methods, the amount of water phase capillary continuity could be different. The fractures produced by the band saw had smoother fracture surfaces which were expected to produce better capillary continuity. However, the dynamic saturation development in Figure 4 and Figure 5 and in Figure 12 in Ref. 6 indicated that the different types of fractures, fine and coarse, had the same influence on the flow paths and the fluid movement across the fractures. These experiments indicated that at the flow rates used in reservoirs the fractures will influence the flow pattern in water-wet chalk. No significant difference was observed for constant flow rate and constant differential pressure waterfloods.

Very good reproducibility was observed between the blocks and also when repeating the experiment on each individual block (Ref. 6). Results for moderately water wet and neutral wet blocks will be published later (Ref. 10).

CONCLUSIONS

1) The experiments demonstrated that radioactive tracers can be conveniently and quantitatively used to follow the 2-D movement of brine when waterflooding relatively large chalk blocks.
2) There appears to be no limitation to the size of the block other than restriction on pressure vessel size and a compromise between accuracy, time and spatial resolution of saturation information.
3) Water movement, during water flooding, was significantly affected by the presence of fractures. The different embedded fracture orientations had different influences on the movement of fluids. However no significant difference between fractures with coarse and fine surfaces was observed.
4) No difference in saturation development was observed between constant flow rate and constant differential pressure waterfloods.
5) During the water flood of the unfractured block and for inlet Block A, in the fractured blocks, the brine saturation was observed as a dispersed front at low S_{wi}, which is different compared to earlier results obtained with relatively high S_{wi}.

6) Although the flow paths were different for the unfractured and fractured blocks, the waterflood endpoint, S_{wf}, and oil production were the same for both configurations. This may be related to the highly water wet state of the chalk.
7) Very good reproducibility of water movement and the final water saturation were observed between the blocks and also when repeating the experiment on each individual block
8) A similar saturation development was observed in two blocks of different chalk materials with different permeability during waterflood.

ACKNOWLEDGMENTS

The authors acknowledge permission to publish the above paper from Phillips Petroleum Company Norway and Co-venturers, including Fina Exploration Norway S.C.A., Norsk Agip A/S, Elf Petroleum Norge A/S, Norsk Hydro Produksjon a.s., Total Norge A/S, Den norske stats oljeselskap a.s., Elf Rex Norge A/S and Saga Petroleum a.s.

REFERENCES

1. Graue, A. and Viksund, B.G., “Imaging Immiscible Two Phase Flow in Low Permeability Chalk - Emphasis on Recovery Mechanisms and Scaling”, presented at the EAPG/AAPG Special Conference on Chalk, Copenhagen, Denmark,(Sept. 7-9, 1994) with an extended abstract printed in the conference proceedings.
2. Graue, A., “Nuclear Tracer Saturation Imaging of Fluid Displacement in Low-Permeability Chalk”, Proc.: SPE Rocky Mountain Regional/Low Permeability Reservoirs Symposium, Denver, CO, USA, (April 26-28, 1993).
3. Viksund, B.G., Hetland, S., Graue, A. and Baldwin, B.A.: "Imaging Saturation during Flow in Fractured Chalk: Emphasizing Recovery Mechanisms, Capillary Continuity and Scaling", presented at the 1996 International Symposium of the Society of Core Analysts, Montpellier, France, (Sept. 8-10, 1996).
4. Torsaeter, O., “An Experimental Study of Water Imbibition in Chalk from the Ekofisk Field”, SPE preprint 12688 presented at the SPE/DOE Fourth Symposium on EOR, Tulsa, OK, (April 1984).
5. Graue, A., Tonheim, E. and Baldwin, B., “Control and Alteration of Wettability in Low-Permeability Chalk”, presented at The 3rd International Symposium on Evaluation of Reservoir Wettability and Its Effect on Oil Recovery, Laramie, Wyoming (Sept., 1995).
6. Viksund, B.G., Graue, A., Baldwin, B. and Spinler, E., "2-D Imaging of waterflooding a Fractured Block of Outcrop Chalk". Presented at 5th Chalk Research Symposium, Reims, France. (7-9 Oct 1996)
7. Lien, J.R., Graue, A. and Kolltveit, K., “A Nuclear Imaging Technique for Studying Multiphase Flow in a Porous Medium at Oil Reservoir Conditions”, Nucl. Instr. & Meth., A271, 693-700 (1988).
8. Graue, A., Kolltveit, K., Lien, J.R. and Skauge, A.: “Imaging Fluid Saturation Development in Long Coreflood Displacements”, SPEFE, Vol.5, No.4, 406-412, (Dec., 1990).
9. Baldwin, B. and Spinler, E., Private Communication of unpublished work.
10. Graue, A., Viksund, B.G., Baldwin, B. and Spinler, E., “Large Scale 2D Imaging of Impacts of Wettability on Oil Recovery in Fractured Chalk”, accepted for presentation at the 1997 SPE 72nd Annual Technical Conference & Exhibition to be held from 05-08 Oct. 1997 in San Antonio.

Table 1. Core data and experimental schedule and flood history of outcrop blocks.

Block	CHP-6		CHP-4		CHD-1	
Outcrop	Rørdal		Rørdal		Dania	
Location	Alborg, Denmark		Alborg, Denmark		Alborg, Denmark	
Length (cm)	19		20		18	
Height (cm)	12		13		11	
Width (cm)	5.5		5.5		5	
Abs. permeability (mD)	3		1.8		67	
Matrix Porosity (%)	45		45		43	
Pore Volume (cm^3)	568		648		434	
Micible Flood # :	1		1		1	
Flow Rate (cm^3/h)	15.5		25		4	
Oilflood # :	1	2	1	2	1	2
Oil Viscosity (cP)	0.92	0.92	0.92	0.92	0.92	0.92
S_{wi} (%PV) [a]	100	72	100	65	100	66
dS_w (%PV) [a]	72	43	73	39	62	29
S_{wf} (%PV) [a]	28	29	27	26	38	37
Endpoint eff. perm. (mD)	1.9	1.9/2.9[b]	1.7	1.6/4.6[b]	59	59/88[b]
Waterflood # :	1	2	1	2	1	2
Block Condition	Whole	Fractured	Whole	Fractured	Whole	Fractured
Cutting		Band Saw		Hand Saw		Hand Saw
S_{wi} (%PV) [a]	28	29	27	26	38	37
dS_w (%PV) [a]	44	43	38	40	28	26
S_{wf} (%PV) [a]	72	72	65	66	66	63
Endpoint eff. perm. (mD)	.6	2.0	.4	.6	15	9
Oil Recovery (%OIP)	62	60	52	54	45	41
Inj. Rate / Const. Pres (cm^3/h / mbar)	6 / -	1 / -	- / 40	- / 40	3.9/-	3.9/-

[a] - Mass Balance
[b] - Before fracturing/After fracturing
S_{wi} - initial water saturation
S_{wf} - final water saturation
dS_w - produced fluid

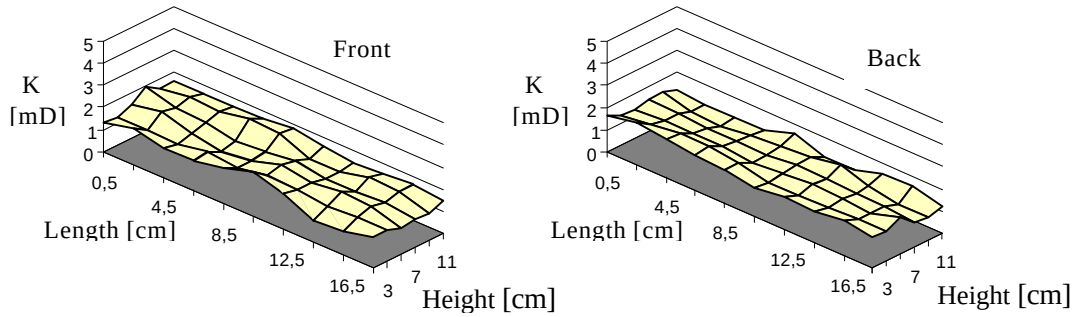

Fig. 1. Air permeability map of Rørdal outcrop chalk block CHP-6.

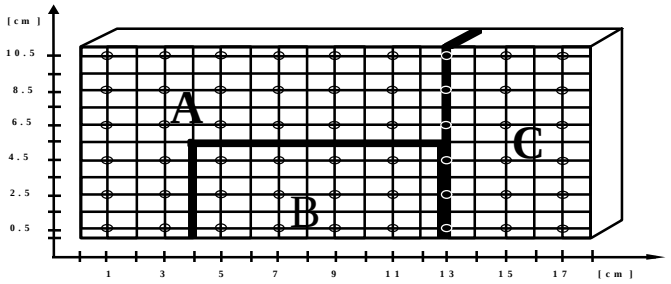

Fig. 2. Outline of fracture network and grid pattern for imaging Block CHD-1.

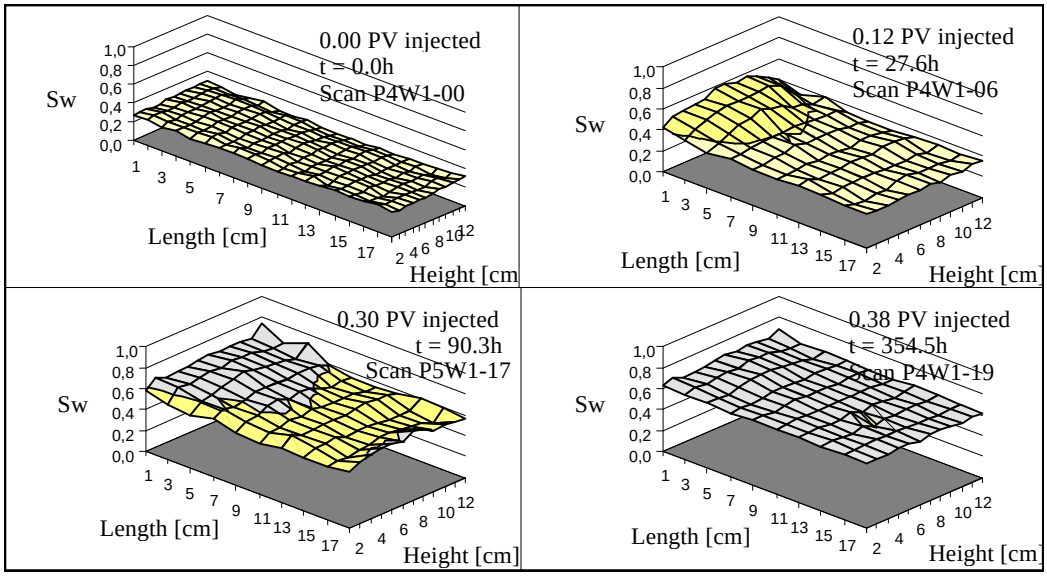

Fig. 3. First waterflood on whole Block CHP-4.

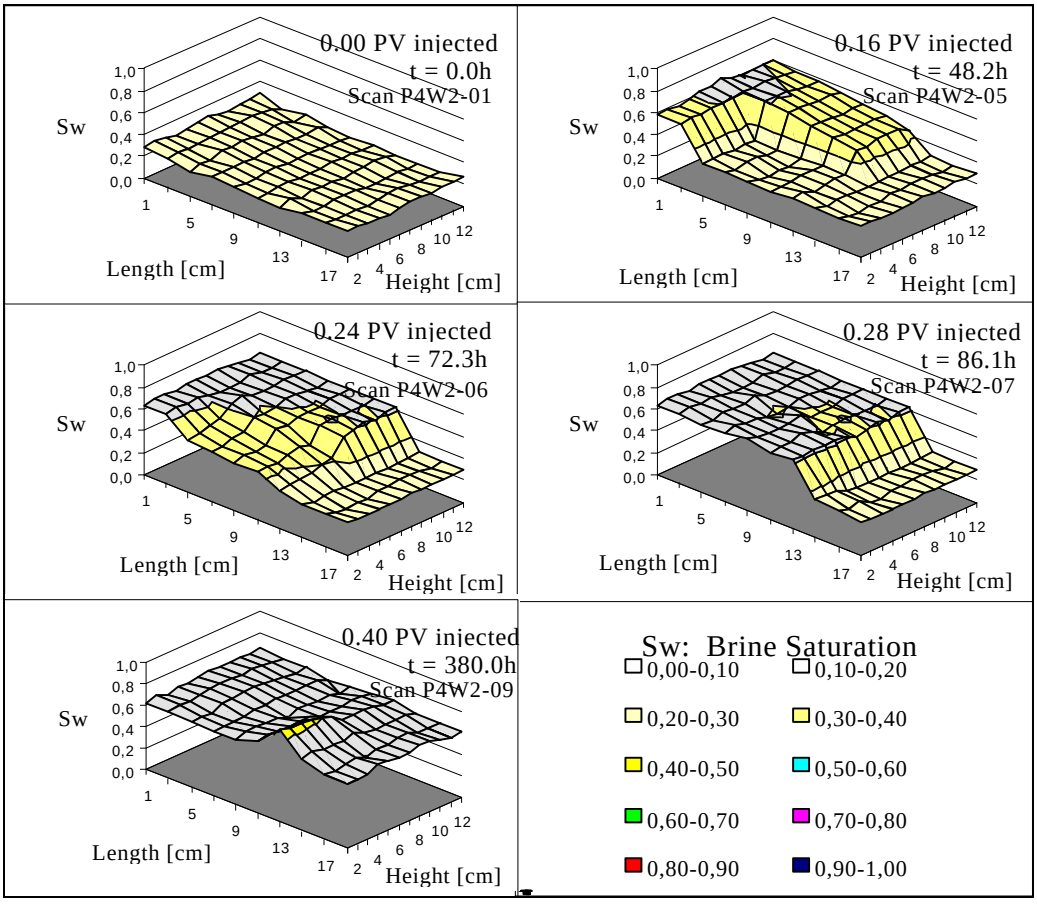

Fig. 4. Second waterflood on fractured Block CHP-4.

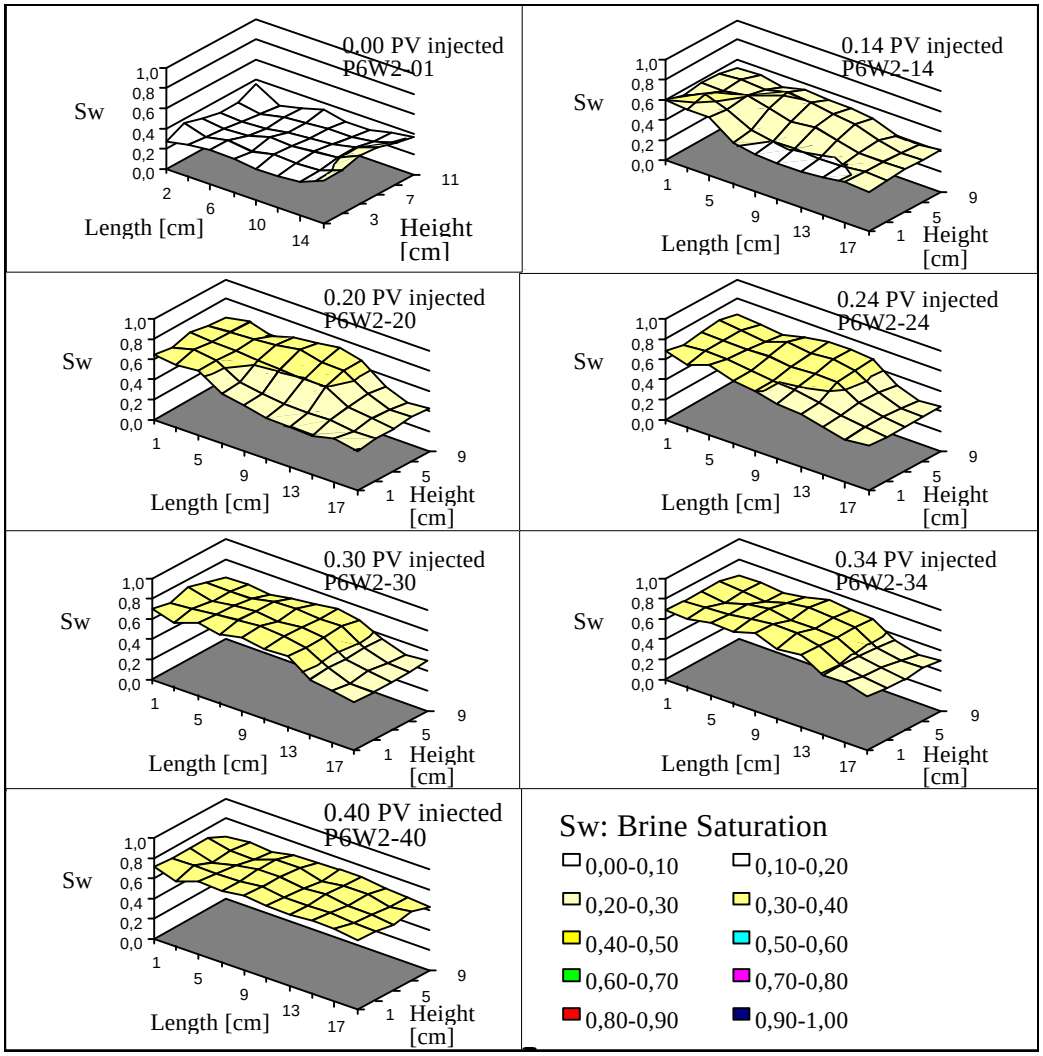

Fig. 5. Second waterflood on fractured Block CHP-6.

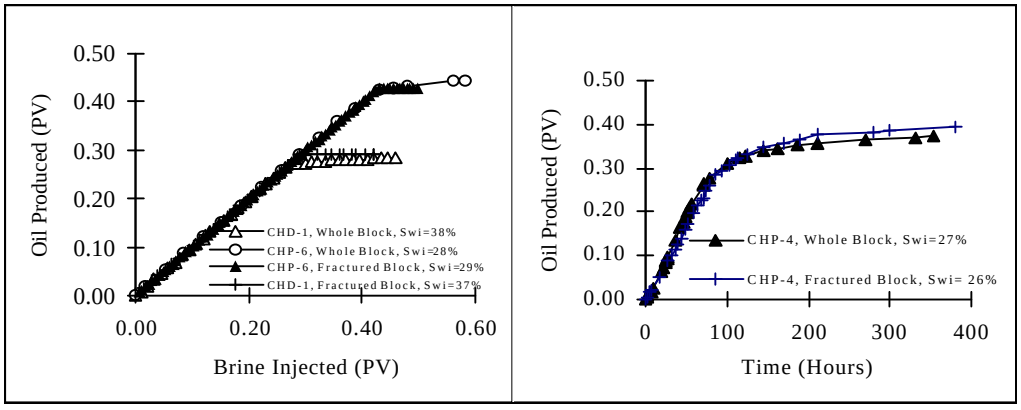

Fig. 6. Effluent profiles for waterflooding whole- and fractured blocks at constant flow rate.

Fig. 7. Effluent profiles for waterflooding of whole- and fractured blocks at constant differential pressure.